CHEMICAL ENGINEERING TRANSACTIONS
VOL. 60, 2017
A publication of AIDIC
The Italian Association of Chemical Engineering
Online at www.aidic.it/cet
Guest Editors: Luca Di Palma, Elisabetta Petrucci, Marco Stoller

ISBN 978-88-95608- 50-1; **ISSN** 2283-9216
DOI: 10.3303/CET1760043

Experimental and Modelling Study of Ionic Selectivity in Carbon Coated Alumina Nanofiber Membranes

Ilya I. Ryzhkov[a]*, Denis V. Lebedev[a], Vera S. Solodovnichenko[a], Alexey V. Shiverskiy[a,c], Michael M. Simunin[a,b], Vladimir A. Parfenov[d]

[a]Institute of Computational Modelling SB RAS, Akademgorodok 50–44, Krasnoyarsk, Russia
[b]Molecular electronics department KSC SB RAS, Akademgorodok 50–44, Krasnoyarsk, Russia
[c]National Research University of Electronic Technology – MIET, Shokin square 1, Zelenograd, Moscow, Russia
[d]Institute of Chemistry and Chemical Technology SB RAS, Akademgorodok 50–24, Krasnoyarsk, Russia
rii@icm.krasn.ru

A novel type of ion-selective membranes, which combine the advantages of ceramic nanofibrous media with good electrical conductivity, is proposed. The membranes are produced from Nafen alumina nanofibers (diameter around 10 nm) by filtration of nanofiber suspension through a porous support followed by drying and sintering. Electrical conductivity is achieved by depositing a thin carbon layer on the nanofibers by CVD. Raman spectroscopy and TEM are used to confirm the carbon structure formation. The average pore size determined by low temperature nitrogen adsorption experiments lies in the range 15–30 nm. Measurements of membrane potential show that the carbon coated membranes acquire high ionic selectivity (transference numbers 0.94 for anion and 0.06 for cation in aqueous KCl). The fixed membrane charge is determined by fitting the experimental data to Teorell–Meyer–Sievers and Space-charge models.

1. Introduction

The interest in membrane separation using ceramic materials has greatly increased over the last decades. Ceramic membranes made from metal oxides offer a number of advantages over polymeric membranes, such as higher thermal and mechanical stability, enhanced chemical and biological resistance, the ease of cleaning, and longer operational lifetime (Li, 2007; Gitis and Rothenberg, 2016). It determines their high potential in such membrane processes as nano-, ultra-, and microfiltration (Garmash et al 1995; Benfer et al 2004; Volkov et al 2008). In ceramic membranes fabricated from granular materials, the solid phase often occupies a large part of the total volume. Its fraction can be essentially reduced by using fibrous materials resulting in membranes with high permeability, low basis weight, and relatively high strength.
In recent years, a unique nanofibrous material Nafen™ has been developed by ANF Technologies. It consists of highly aligned γ–phase alumina nanofibers with the diameter of 10–15 nm and length more than 100 mm. The material offers a high specific surface of 155 m^2/g. Dispersion of Nafen nanofibers in water provides stable colloidal systems (Saunders et al 2015) perspective for the preparation of porous ceramic membranes. Membranes for ultrafiltration were produced by dispersion of Nafen nanofibers in water, filtering through a coarse mesh to obtain the membrane precursor, drying, and sintering (Su et al 2012, Su and Clyne 2016).
We believe that the combination of ceramic nanofibers and carbon materials is promising for the preparation of membranes with selective ion transport. The carbon surface layer can form a wide range of functional groups, which could be utilized to control the membrane selectivity. The use of electroconductive nanofibers opens new ways for producing membranes with switchable ion-transport selectivity. Such selectivity was previously realized by applying a prescribed potential to gold-covered pores of track–etched polymeric membranes (Nishizawa 1995). However, these membranes had a very low porosity (less then 1%) and, consequently, permeability. In this work, we describe a novel type of ion-selective membranes based on Nafen alumina nanofibers, which combine the advantages of ceramic nanofibrous media and good electrical conductivity. The physico-chemical characterization of prepared membranes is performed and their ion-selective properties are investigated. The measured membrane potentials are fitted by the Nernst equation

Please cite this article as: Ryzhkov I., Lebedev D., Solodovnichenko V., Shiverskiy A., Simunin M., Parfenov V.A., 2017, Experimental and modelling study of ionic selectivity in carbon coated alumina nanofiber membranes, Chemical Engineering Transactions, 60, 253-258
DOI: 10.3303/CET1760043

with transference, Teorell-Meyer-Sievers model and Space charge model to determine the fixed membrane charge.

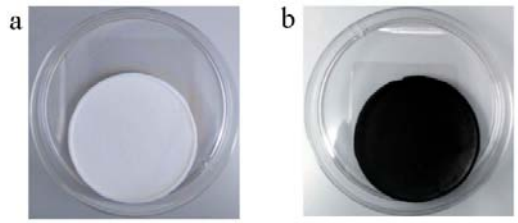

Figure 1: Top view of Nafen membrane before (a) and after (b) deposition of carbon by CVD method.

2. Experimental

2.1. Membrane preparation

The membranes are prepared from Nafen supplied by ANF Technology (www.anftechnology.com) in the form of nanofiber blocks. The nanofibers were dispersed in de-ionized water (Nafen:water 1:200) and agitated with a magnetic stirrer for 30 minutes followed by 15 minutes of ultrasonic treatment (UZDN–2T, 22 kHz, 400 W). The suspension was filtered through the rough Teflon filter (pore size of ~0.6 μm) and dried in air. Then membrane was sintered at 800 °C during 4 hours to ensure its structural stability in aqueous solutions. The produced membrane is a circular disc with the diameter of 35 mm and thickness of about 400 μm (Fig. 1a).
Chemical vapor deposition (CVD) was used to form carbon layers on membranes. The synthesis was conducted in the reactor at 900 °C (heating rate of 20–30 °C/min) in propane/nitrogen mixture (1/15) with the total flow rate of 4000 cm^3/min during 60 seconds. The mass gain after CVD was around 15 %. The sample was slowly cooled to 150 °C in the atmosphere of nitrogen. The resulting membrane is shown in Fig. 1b. The samples with and without deposited carbon will be referred to as C–Nafen membrane and Nafen membrane, respectively.

2.2. Membrane characterization

Scanning electron microscopy (SEM) and transmission electron microscopy (TEM) were used to characterize the morphology of membranes prepared from alumina nanofibers. The SEM was performed by the Hitachi scanning microscope S–5500 (Japan) operating at 3 kV. The TEM images were obtained by the Hitachi HT–7700 instrument (Japan) with an accelerating voltage of 100 kV.
Low temperature nitrogen adsorption experiments were performed at ASAP–2420 (Micromeritics, USA) for membrane pore and surface area characterizations. Textural characteristics calculations of materials under consideration were realized with BET, BJH, and t–plot models.
Raman spectra in the backscattering geometry were recorded with the Horiba Jobin Yvon 64000 triple spectrometer (France) equipped with a liquid nitrogen cooled charge coupled device detection system in subtractive dispersion mode. Ar+ ion laser Spectra–Physics Stabilite 2017 with λ=514.5 nm and power 100–400 μW on a sample was used as an excitation light source.

2.3. Membrane potential measurement

The ion permselectivity of prepared membranes was studied by measuring the potential difference between two electrolyte solutions with different concentrations separated by a membrane (Fig. 2). The laboratory made electrochemical cell consists of two compartments, between which the membrane is clamped. In each half-cell, reference 4.2 M Ag/AgCl electrode is located. Electrodes are connected to the potentsiostat PI–50Pro (ELINS, Russia), which measures the cell electromotive force (EMF) in 'broken circuit potential measurement' mode. The measurements were performed in KCl aqueous solution. First, the solution with fixed concentration C_R was placed in both half–cells. The system was kept at room temperature of 25 °C during 12 hours.

The measurements were performed by increasing the concentration of KCl in the left half–cell C_L by consecutive addition of the KCl concentrate (1M or 4.2M). For large values of C_L (> 1M), the solution was completely replaced with that of higher concentration. After each addition / replacement, the system was allowed to equilibrate during 30 min. Then the cell EMF was measured. After each series of experiments, the membrane was placed in deionized water for 24 hours to remove the rest of electrolyte solution from the pores.

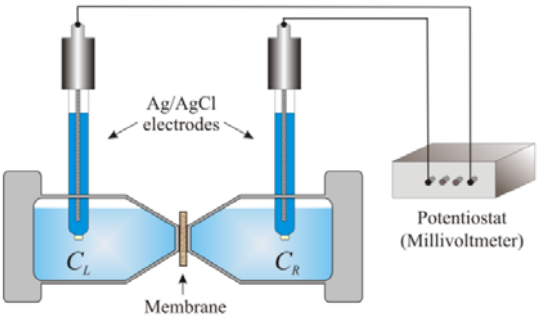

Figure 2: The scheme of electrochemical cell and experimental setup.

3. Theoretical

3.1. Nernst equation with transference

A simplified approach to interpreting the potential difference between two half–cells separated by a membrane (Figure 2) is provided by the equation (Strathmann 2011)

$$\Phi = 2.303\,(t_+ - t_-)\frac{R_g T}{F} log\frac{a_L}{a_R}, \qquad (1)$$

where R_g is the ideal gas constant, T is the temperature, F is the Faraday constant, a_L and a_R are the activities of solutions in the left and right half-cells, respectively. They are related to concentrations through the activity coefficients $a_{L,R} = \gamma(C_{L,R})C_{L,R}$ taken from tabulated data (Lide 2003–2004). In equation (1), t_+ and t_- are transference numbers of anions and cations in membrane, respectively ($t_+ + t_- = 1$). The transference numbers are found by determining the slope of Φ vs $log(a_L / a_R)$ from the experimental data.

3.2. Theorell-Meyer-Sievers model

According to the theory of Teorell, Meyer and Sievers (TMS theory), the total potential difference $\Phi = \Phi_R - \Phi_L$ across the membrane for binary monovalent electrolyte is given by (Tanaka 2015)

$$\Phi = \frac{R_g T}{F}\left[\ln\frac{C_L}{C_R}\left(\frac{-X+\sqrt{X^2+4C_R^2}}{-X+\sqrt{X^2+4C_L^2}}\right) - D\ln\left(\frac{-DX+\sqrt{X^2+4C_R^2}}{-DX+\sqrt{X^2+4C_L^2}}\right)\right], \quad D = \frac{D_+ - D_-}{D_+ + D_-}, \qquad (2)$$

where the first and second terms represent the contributions from Donnan potential and diffusion potential, respectively. In formula (2), $D_\pm$ are the diffusion coefficients of positive and negative ions and X is the volume density of membrane fixed charge, which is related to the surface charge density σ by the formula

$$X = \frac{2\sigma}{FR}, \qquad (3)$$

where R is the pore radius. Anion– and cation–selective membranes correspond to the cases $X > 0$ and $X < 0$, respectively. The volume density of fixed charge X is determined by fitting the experimentally measured values of Φ at constant C_R and varying C_L to formula (2).

3.3. Space-charge model

In this model, the flow and ion transport in the pore with radius R and length L are described by the Navier-Stokes, Nernst-Planck and Poisson equations, which are simplified and reduced to a special form (Peters et al 2016). Let us introduce dimensionless variables by choosing the characteristic scales of length R and L (in radial and longitudinal directions, respectively), concentration $C_{ref} = 10^{-3}\mathrm{M}$, electric potential $R_g T / F$, ion fluxes $D_+ C_{ref} / L$, velocity D_+ / L, pressure $C_{ref} R_g T$, and surface charge density $\varepsilon\varepsilon_0 R_g T / FR$. Here ε is the relative dielectric permittivity, and ε_0 is the dielectric constant. The dimensionless electric potential φ, ion concentrations $c_\pm$, and pressure p in the Space-charge model are written as

$$\varphi(r,x) = \phi_v(x) + \psi(r,x), \qquad c_\pm(r,x) = c_v(x)exp(\mp\psi(r,x)), \qquad p(r,x) = p_v(x) + 2c_v(x)cosh(\psi(r,x)). \qquad (4)$$

Here ϕ_v, c_v, p_v are the so-called virtual quantities. The part of electric potential $\psi(r,x)$ satisfies the Poisson equation with boundary conditions of fixed surface charge at the pore wall and symmetry at the pore axis

$$\frac{1}{r}\frac{\partial}{\partial r}\left(r\frac{\partial\psi(r,x)}{\partial r}\right)=\frac{c_v(x)}{\lambda_{ref}^2}sinh(\psi(r,x)),\qquad \frac{\partial\psi(1,x)}{\partial r}=\sigma',\qquad \frac{\partial\psi(0,x)}{\partial r}=0, \tag{5}$$

where σ' is the dimensionless surface charge density and $\lambda_{ref}=R^{-1}\sqrt{\varepsilon\varepsilon_0R_gT\,/\,2F^2C_{ref}}$ is the dimensionless Debye length. The virtual quantities satisfy the following system of ODE:

$$\frac{dp_v}{dx}=L'_{11}J_V+L'_{12}J_I+L'_{13}J_C,\qquad \frac{1}{c_v}\frac{dc_v}{dx}=L'_{12}J_V+L'_{22}J_I+L'_{23}J_C,\qquad \frac{d\phi_v}{dx}=L'_{13}J_V+L'_{23}J_I+L'_{33}J_C. \tag{6}$$

Here J_V is the cross-sectionally averaged velocity, $J_I=J_++J_-$ is the total averaged ion flux, and $J_C=J_+-J_-$ is the averaged ion current. Further, $L'=\{L'_{ij}\}=-L^{-1}$ is a matrix. The components of $L=\{L_{ij}\}$ are calculated from solution to problem (5). In contrast to Peters et al 2016, we take into account different ion diffusion coefficients.

We apply the Space-charge model to describing the ion transport in diffusion cell, where a cylindrical pore connects two reservoirs with different (here dimensionless) concentrations C_L and C_R. There is no electric current ($J_C=0$). The pressures in both reservoirs are equal and are taken to be zero: $p(r,0)=p(r,1)=0$. The potential in the left reservoir is $\varphi(r,0)=0$. Using the second equation in (6) in the form

$$dx=\frac{dc_v}{dc_v\,/\,dx}=\frac{dc_v}{c_v(L'_{12}J_V+L'_{22}J_I)},$$

we substitute it into the first and third equations in (6) and integrate them from $x=0$ to $x=1$. Taking into account boundary conditions (see also (4) and note that $\psi(r,x)=0$ in the reservoirs)

$$x=0:\quad p_v=-2C_L,\ c_v=C_L,\ \phi_v=0;\qquad x=1:\quad p_v=-2C_R,\ c_v=C_R,\ \phi_v=\Phi,$$

we find

$$\int_{C_R}^{C_L}\frac{L'_{11}+L'_{12}J}{c_v(L'_{12}+L'_{22}J)}dc_v+2(C_L-C_R)=0,\qquad \Phi=-\int_{C_R}^{C_L}\frac{L'_{13}+L'_{23}J}{c_v(L'_{12}+L'_{22}J)}dc_v, \tag{7}$$

where $J=J_I\,/\,J_V$. The membrane potential is calculated as follows. First, problem (5) is solved in the range of c_v values from C_R to C_L. Then the coefficients $L'_{ij}(c_v)$ are calculated. The ratio of fluxes J is found by numerical solution of first equation in (7). Membrane potential Φ is calculated from the second formula in (7).

4. Results and discussion

4.1. Membrane characterization

According to SEM and TEM images (Fig. 3), resulting membranes consist of randomly oriented alumina nanofibers with high aspect ratio (~100) and small diameter (~ 8 nm) covered by a few carbon layers with the total thickness around 1–2 nm. The Raman spectrum of C–Nafen membrane is shown at Fig. 4. The sharp peaks at 1325 cm^{-1} and 1590 cm^{-1} corresponds to the D (disorder) peak and G (graphitic) peak of the carbon. The relative intensity of D and G peaks (I_D/I_G) in C–Nafen membrane spectrum is approximately 1.035. Along with broadening of G peak and its shifting to 1590 cm^{-1}, it indicates the formation of disordered structures of amorphous carbon during CVD synthesis. A wide 2D peak, which is related to the carbon layer structure, is observed at 2700–3000 cm^{-1}. According to the low-temperature nitrogen adsorption measurements, the deposition of carbon decreases the average pore diameter and porosity of membranes. The pore size distribution maximum shifts from 28 nm for Nafen membrane to 16 nm for the C–Nafen membrane. The total volume of pores decreases from 0.76 cm^3/g (Nafen membrane) to 0.49 cm^3/g (C–Nafen membrane), while the specific area decreases from 146 m^2/g to 107 m^2/g, respectively. The porosity calculated from textural parameters is 75 % for Nafen and 62 % for C–Nafen membranes. The permeability estimated on the basis of Kozeny-Carman equation is 64 $l{\cdot}m^{-2}h^{-1}bar^{-1}$ for Nafen membranes and 18 $l{\cdot}m^{-2}\ h^{-1}\ bar^{-1}$ for C–Nafen membranes. It is comparable with the permeability of alumina nanofiber membranes (Su et al 2012) and carbon modified porous anodic alumina membranes (Mattia 2012).

4.2. Ionic selectivity

We have studied the ionic selectivity of Nafen and C–Nafen membranes by measuring the potential difference between two half–cells with different KCl concentrations. The concentration in the right half–cell was fixed at $C_R=1$ mM or $C_R=10$ mM, while the concentration in the left half–cell was varied from C_R up to 4.2 M.

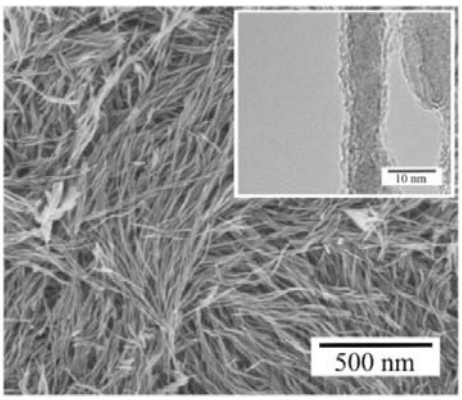

Figure 3: SEM image of the C–Nafen membrane and TEM image of nanofibers (at the insert).

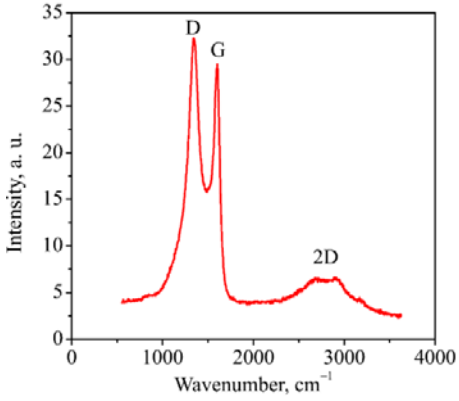

Figure 4: Raman spectrum of C–Nafen membrane.

The results were fitted by Nernst equation (1), TMS model (2), and Space-charge model (Section 3.3). The pore radii $R = 14$ nm and $R = 8$ nm were taken for the Nafen and C–Nafen membranes (see Section 4.1).

The Nafen membranes consist of γ–Al_2O_3. Its surface charge is determined by the solution pH, which was 6–7 during the measurements. In this case, the positive charge should accumulate on the surface of alumina nanofibers due to adsorption of cations (Tschapek et al 1976). The measured membrane potential for Nafen membranes was negative and small in magnitude (10–20 mV), which indicates weak anion selectivity.

The deposition of carbon changes the interaction of membrane with the electrolyte solution. The ions preferably bind on the structural defects of carbon layer. Modelling of Na^+ and Cl^- adsorption reveals the preferable adsorption of alkali metal on carbon surface (Mpourmpakis and Froudakis 2006). Thus, one can expect that after deposition of carbon the membrane selectivity would greatly increase due to strong interaction between carbon surface and K^+ ion. The carbon coating also decreases the pore size providing stronger double layer overlap and enhancing selectivity.

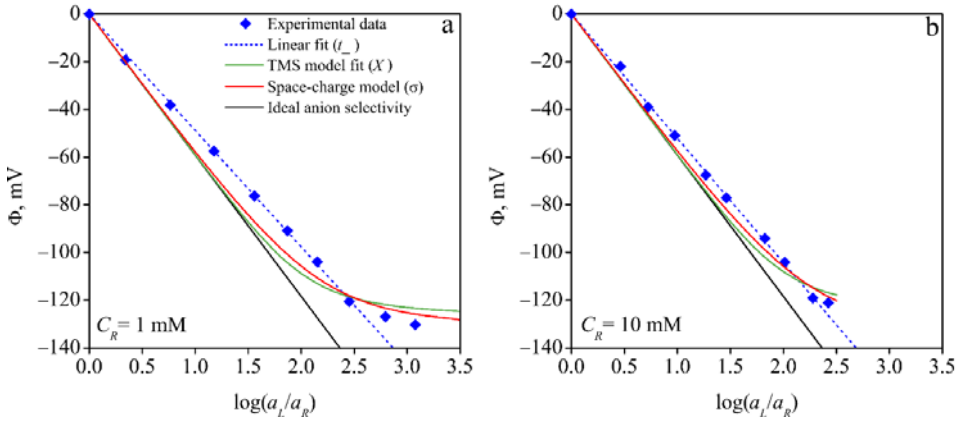

Figure 5: The dependence of membrane potential Φ on the logarithm of activities ratio for the C–Nafen membrane. The concentration in the right half–cell is $C_R = 1$ mM (a) and $C_R = 10$ mM (b).

The membrane potential for the C–Nafen membrane shown in Figure 5 gives evidence of high anion selectivity. The data are well fitted by Nernst-Planck equation (1) with high anion transference numbers, see Table 1. The fit by TMS model (2) is not so good, but still can be used to estimate the membrane fixed charge. The Space-charge (SC) model provides a better fit to the data. The determined surface charge is 1.5–2.3 times higher than that for the TMS model. Note that SC model takes into account radial variations of potential and concentrations, while TMS model assumes complete double-layer overlap. In fact, the Debye length decreases from the pore entrance to the pore exit due to the concentration change from larger C_L to smaller C_R.The increase of concentration from $C_R = 1$ to $C_R = 10$ mM decreases the Debye length, which should reduce the ionic selectivity. At the same time, it leads to the increase of fixed charge by ~10 times, which enhances the ionic selectivity. For the C–Nafen membrane, the former effect slightly overcomes the latter one, which results in higher anion transference number for the increased concentration, see Table 1.

Table 1: Transference numbers, volume density X and surface density σ of fixed membrane charge for different concentrations C_R in the right half–cell.

Membrane		Nernst equation		TMS model		Space-charge model
	C_R, mM	t_+	t_-	X, mM	σ, 10^{-3} C m^{-2}	σ, 10^{-3} C m^{-2}
C–Nafen	1	0.09	0.91	116.1	44.8	69.4
C–Nafen	10	0.06	0.94	1021.1	394.0	896.0

5. Conclusion

A novel type of ion-selective membranes, which combine the advantages of ceramic nanofibrous media with good electrical conductivity, is proposed. The latter is achieved by depositing a thin carbon layer on the matrix of alumina nanofibers by chemical vapor deposition. Raman spectroscopy and TEM confirm the carbon structure formation. Measurements of membrane potential show that the carbon coated membranes acquire high anion selectivity (transference numbers 0.94 for anion and 0.06 for cation in aqueous KCl). The fixed membrane charge results from the adsorption of cations on the defects of carbon structure. It is determined by fitting the experimental data to Teorell–Meyer–Sievers and Space-charge models. The fixed membrane charge increases proportionally to electrolyte concentration. The potential applications of produced membranes include nano- and ultrafiltration, separation of charged species, and switchable ion-transport selectivity.

Acknowledgement

This work is supported by the Russian Science Foundation, Project 15–19–10017. The physicochemical analysis of materials was carried out at Krasnoyarsk Scientific Center of Shared Facilities.

References

Benfer S., Árki P., Tomandl G., 2004, Ceramic membranes for filtration applications – preparation and characterization, Adv Engineer Materials 6, 495–500.

Galama A.H., Post J.W., Hamelers H.V.M., Nikonenko V.V., Biesheuvel P.M., 2016, On the origin of the membrane potential arising across densely charged ion exchange membranes: how well does the Teorell–Meyer–Sievers theory work? J Membr Sci & Res 2, 128–140.

Garmash E.P., Kryuchkov Y.N., Pavlikov V.N., 1995, Ceramic membranes for ultra- and microfiltration (review), Glass and Ceramics 52, 150–152.

Gitis V., Rothenberg G., 2016, Ceramic membranes: new opportunities and practical applications, Wiley–VCH, Weinheim, Germany.

Li K., 2007, Ceramic membranes for separation and reaction, John Wiley & Sons, Chichester, England.

Lide D.R., 2003-2004, Handbook of Chemistry and Physics, 84th Edition. CRC press, Boca Raton.

Mattia D., Leese H., Lee K.P., 2015, Carbon nanotube membranes: from flow enhancement to permeability, J. Membr. Sci., 475, 266–272.

Mpourmpakis G., Froudakis G., 2006, Why alkali metals preferably bind on structural defects of carbon nanotubes: A theoretical study by first principles, J Chem Phys. 125, 204707.

Nishizawa M., Menon V.P., Martin C.R., 1995, Metal nanotubule membranes with electrochemically switchable ion–transport selectivity, Science 268, 700–702.

Peters P.B., Van Roij R., Bazant M.Z., Biesheuvel P.M. 2016, Analysis of electrolyte transport through charged nanopores, Phys Rev E 93, 053108.

Saunders Z., Noack C.W., Dzombak D.A., Lowry G.V., 2015, Characterization of engineered alumina nanofibers and their colloidal properties in water, J Nanopart Res 17, 140.

Strathmann H., 2011, Introduction to membrane science. Wiley–VCH, Weinheim, Germany.

Su V., Terehov M., Clyne B., 2012, Filtration performance of membranes produced using nanoscale alumina fibers (NAF), Adv Engineer. Materials 14, 1088–1096.

Su V.M.T., Clyne T.W. 2016, Hybrid filtration membranes incorporating nanoporous silica within a nanoscale alumina fiber scaffold, Adv Engineer Materials 18, 96–104.

Tanaka Y., 2015, Ion exchange membranes: fundamentals and applications. Elsevier, Amsterdam.

Tschapek M., Wasowski C., Torres Sanchez R.M., 1976, The p.z.c. and i.e.p. of γ-Al_2O_3 and TiO_2, J Electroanal Chem. 74, 167–176.

Volkov V.V., Mchedlishvili B.V., Roldugin V.I., Ivanchev S.S., Yaroslavtsev A.B., 2008, Membranes and nanotechnologies, Nanotechnologies in Russia 3, 656–687.